

Smaller Sulfur Molecules Promise Better Lithium–Sulfur Batteries

Sen Xin,[†] Lin Gu,[§] Na-Hong Zhao,[‡] Ya-Xia Yin,[†] Long-Jie Zhou,[‡] Yu-Guo Guo,^{*,†} and Li-Jun Wan^{*,†}

[†]Key Laboratory of Molecular Nanostructure and Nanotechnology and Beijing National Laboratory for Molecular Sciences, Institute of Chemistry, Chinese Academy of Sciences, and [§]Beijing National Laboratory for Condensed Matter Physics, Institute of Physics, Chinese Academy of Sciences, Beijing 100190, P.R. China

[‡]Bosch Research & Technology Center, Asia Pacific District China, Bosch (China) Investment Ltd., Shanghai 200335, P.R. China

Supporting Information

ABSTRACT: The lithium–sulfur battery holds a high theoretical energy density, 4–5 times that of today's lithium-ion batteries, yet its applications have been hindered by poor electronic conductivity of the sulfur cathode and, most importantly, the rapid fading of its capacity due to the formation of soluble polysulfide intermediates (Li_2S_n , $n = 4-8$). Despite numerous efforts concerning this issue, combatting sulfur loss remains one of the greatest challenges. Here we show that this problem can be effectively diminished by controlling the sulfur as smaller allotropes. Metastable small sulfur molecules of S_{2-4} were synthesized in the confined space of a conductive microporous carbon matrix. The confined S_{2-4} as a new cathode material can totally avoid the unfavorable transition between the commonly used large S_8 and S_4^{2-} . Li–S batteries based on this concept exhibit unprecedented electrochemical behavior with high specific capacity, good cycling stability, and superior rate capability, which promise a practicable battery with high energy density for applications in portable electronics, electric vehicles, and large-scale energy storage systems.

There is no doubt that the pursuit of advanced energy storage devices with higher energy densities is critical for powering our future society.¹ Among the best candidates for next-generation high-energy-storage systems, metal–sulfur batteries, such as Li–S, Na–S, and Mg–S,^{1b,2} hold high theoretical energy densities, making them especially attractive. Of these, the Li–S battery has the highest theoretical energy density of 2567 W h kg^{-1} , calculated on the basis of the Li anode (~ 3860 mA·h/g) and the S cathode (~ 1675 mA·h/g), making it a promising choice for the next generation of high-energy rechargeable batteries.^{1b,3}

The application of Li–S batteries suffers from two major issues. One involves with the use of lithium metal as anode, which may raise safety concerns for practical applications due to the growth of lithium dendrite. To address this, replacement of the Li anode with other anode materials, such as Si and Sn, to pair with a Li_2S cathode provides a feasible way to improve the battery's safety.⁴ The other issue lies in the sulfur cathode. It is known that a Li–S battery with a cyclooctasulfur (cyclo- S_8) cathode usually discharges stepwise, with two plateaus in its voltage profile.^{3,5a,b} At the first plateau (~ 2.3 V vs Li^+/Li), sulfur is reduced from S_8 to S_4^{2-} , during which various electrolyte-soluble polysulfides (Li_2S_n , $n = 4-8$) form. The second plateau (~ 1.95 V vs Li^+/Li)

corresponds to the transformation from Li_2S_4 to insoluble Li_2S_2 and finally Li_2S .⁵

The performance of the Li–S battery is therefore limited by the insulating problem with sulfur and the dissolution and shuttling problem with polysulfides in liquid electrolyte.³ Many efforts have been made to improve the performance of sulfur, including the use of various conducting substrates and new electrolytes, e.g., solid-state and ionic liquid types.^{1b,6} Though the former leads to improved electrical conductivity, it does not solve the intrinsic problem with dissolution of polysulfides due to the contained cyclo- S_8 molecules. The latter, intended to relieve the dissolution problem of polysulfides, suffers from the low ionic conductivity of electrolyte at room temperature.

Herein, we propose and realize a new strategy: using small sulfur allotropes S_{2-4} (S_2 , S_3 , and S_4) for high-performance Li–S batteries. Metastable small sulfur molecules have been confined in a microporous carbon (MPC) matrix with pore size of ~ 0.5 nm, revealed by an advanced spherical aberration imaging technique. The confined small S_{2-4} molecules avoid the unfavorable transition between S_8 and S_4^{2-} during discharging/charging and typically give a single long output plateau at ~ 1.9 V. A sulfur–carbon composite containing S_{2-4} molecules shows admirable electrochemical properties in terms of specific capacity, cycling stability, and high rate capability and promises a practical Li–S battery with high energy density.

A composite carbon matrix with a core/porous-sheath structure is designed for subsequent sulfur accommodation (Figure S1). Briefly, multiwalled carbon nanotubes (CNTs, average diameter = 50 nm, Figure S2a) are used as the starting materials and then coated with a MPC layer via a solution-based method. The transmission electron microscopy (TEM) image of the product in Figure 1a shows that the as-obtained CNT@MPC has a coaxial structure with a CNT core and a MPC sheath with a thickness of ~ 100 nm. The mean diameter of the nanocable is ~ 250 nm, further confirmed by the scanning electron microscopy (SEM) image in Figure S2b. From the annular bright-field (ABF) image taken by a scanning transmission electron microscope (STEM), the sizes of the micropores in the MPC layer are measured to be ~ 0.5 nm (Figure 1b). The pore structure of CNT@MPC is further characterized by Type I nitrogen adsorption/desorption isotherms with a specific surface area of 936 m^2/g by the Brunauer–Emmett–Teller (BET) method and a narrow pore size distribution of ~ 0.5 nm by the

Received: August 17, 2012

Published: October 26, 2012

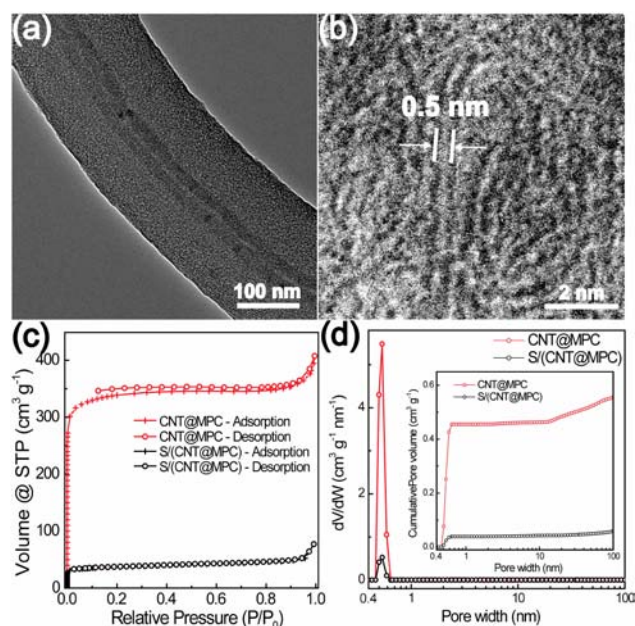


Figure 1. Structural characterizations of CNT@MPC. (a) TEM image of a CNT@MPC nanocable. (b) ABF-STEM image showing the carbon channels in the coating layer, in which dark gray part represents the carbon wall, while light gray represents the carbon channel. (c) N_2 adsorption/desorption isotherms and (d) pore size distribution plots obtained using the DFT method of the CNT@MPC and S/(CNT@MPC); insets show the cumulative pore volumes.

Density Functional Theory (DFT) method (Figure 1c,d), consistent with the above ABF-STEM observation. The cumulative pore volume for the micropores <0.6 nm is calculated to be 0.46 cm^3/g (inset of Figure 1d), which corresponds to a theoretical loading of 49 wt% sulfur in the micropores, based on the density of sulfur (2.07 g/cm^3).

Upon heating of the mixture of sulfur and CNT@MPC (Figure S2c), sulfur diffuses as chain-like molecules into the MPC layer to form the sulfur–carbon composite (S/(CNT@MPC), Figure S2d). X-ray diffraction patterns taken during the sulfur loading process reveal the disappearance of sulfur peaks after heating, indicating a fine dispersion of sulfur into the carbon substrate (Figure S3). A significant decrease in BET surface area is seen after sulfur introduction (from 936 to 82 m^2/g), accompanied by a sharp decrease of the intensity at pore size of 0.5 nm (inset of Figure 1c). The micropore volume decreases to <0.04 cm^3/g , further proving the migration of sulfur into the carbon micropores. Figure 2a shows the TEM image of S/(CNT@MPC), in which the cable-like structure remains after heating. In the HRTEM image of S/(CNT@MPC), only the lattice strings of multiwalled CNTs ($d = 0.34$ nm, corresponding to the (002) crystalline planes) are observed, with no indication of crystalline sulfur in the MPC layer (Figure 2b). However, elemental mapping reveals a uniform distribution of sulfur in the MPC layer (Figure 2d–f). The ABF-STEM image taken from the MPC region shows that short-chain-like sulfur molecules including S_{2-4} are well dispersed in the micropores of MPC (circled in Figure 2c). The S/(CNT@MPC) contains ~ 40 wt% S, as determined by both elemental analysis (40.2 wt%) and energy-dispersive X-ray (EDX) analysis (39.8 wt%, Figure S4a).

Theoretical calculations were performed on different sulfur allotropes to study the existing form of sulfur in the carbon channels, adopting the covalent radius of sulfur is as the radius of

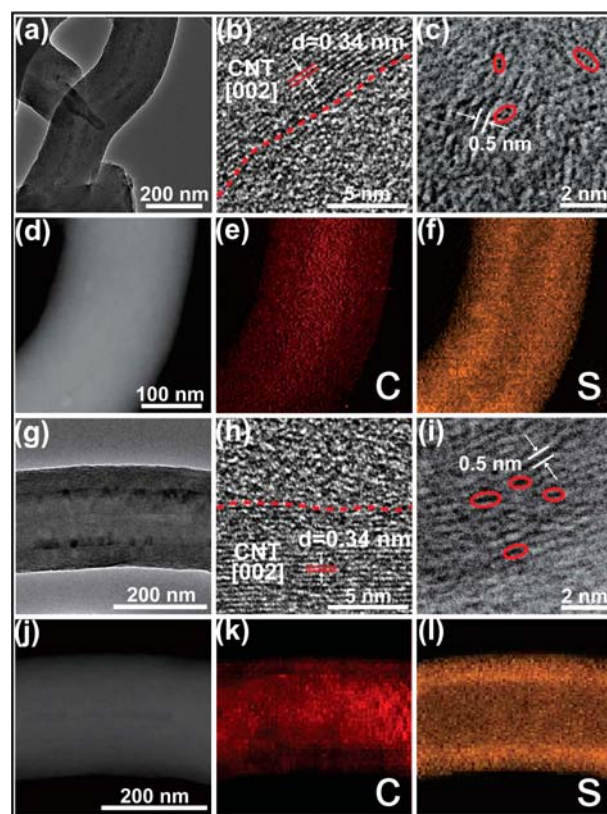


Figure 2. Structural characterization of S/(CNT@MPC) before and after 200 cycles at 0.1 C: (a) TEM, (b) HRTEM, (c) ABF-STEM, (d) annular dark-field TEM, and EDX elemental mappings of (e) carbon and (f) sulfur of the S/(CNT@MPC) nanocable before use; (g) TEM, (h) HRTEM, (i) ABF-STEM, (j) annular dark-field TEM, and EDX elemental mappings of (k) carbon and (l) sulfur of the S/(CNT@MPC) nanocable after use. Black and gray parts represent sulfur and carbon, respectively, in the ABF-STEM images taken from the MPC layer (c, i).

a sulfur atom due to its zerovalent nature in S/(CNT@MPC) (Figure S5). It is found that small sulfur allotropes with chain-like structure, S_{2-4} , have at least one dimension <0.5 nm, while for cyclo-sulfur molecules S_{5-8} , their sizes in at least two dimensions are >0.5 nm (Figure S6). In view of the micropore size of 0.5 nm, only small S_{2-4} molecules can be accommodated in the micropores of MPC, while the large S_{5-8} molecules cannot be stored. In this way, the chain-like sulfur molecules in the carbon micropores could not transform to the large S_8 rings but remain as S_{2-4} molecules. Though it is hard to capture the Raman signals of the confined S_{2-4} molecules due to the interference of the carbon matrix,⁷ the disappearance of the typical Raman peaks of cyclo- S_8 indicates different sulfur forms in S/(CNT@MPC) (Figure S7a).^{6d}

The S/(CNT@MPC) was assembled into Li–S batteries to test the electrochemical behaviors of these small sulfur molecules. For comparison, a sulfur–carbon composite containing cyclo- S_8 was also tested, synthesized by mixing sulfur powder and carbon black (S/CB) with the same sulfur content, 40 wt%. Figure 3a compares the initial galvanostatic discharge/charge (GDC) voltage profiles of the two composites cycled at 0.1 C (167 mA/g based on sulfur mass, same below) in a glyme-based electrolyte of 0.5 M lithium bis(trifluoromethanesulfonyl)imide in tetra(ethylene glycol) dimethyl ether, which has been reported to be a good solvent of polysulfides.^{1b} During the initial discharging process, S/CB exhibits a discharge capacity of 625

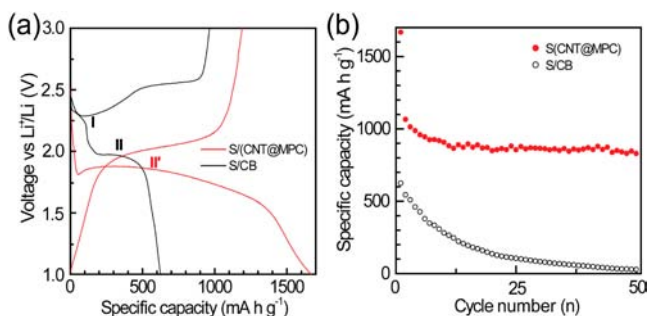


Figure 3. Electrochemical properties in glyme-based electrolyte. (a) Initial GDC voltage profiles and (b) cycling performances of S/(CNT@MPC) and S/CB at 0.1 C.

(250) mA·h/g (for a convenient discussion throughout this paper, the value in parentheses refers to the capacity based on the total mass of the composite, and the one outside refers to the capacity based on sulfur) with two plateaus at 2.3 (Plateau-I) and 1.95 V (Plateau-II), corresponding to the transitions from S_8 to S_4^{2-} and from S_4^{2-} to S^{2-} , respectively, which are consistent with the reported electrochemical behavior of cyclo- S_8 .^{3,5a,b} The initial charging of S/CB also brings two plateaus in the voltage profile and an abnormal Coulombic efficiency of 154%, which indicates a significant dissolution of polysulfides during the process. In the case of S/(CNT@MPC), a novel electrochemical behavior is observed, which shows a large initial discharge capacity of 1667 (666) mA·h/g with only the single Plateau-II at ~1.85 V. This behavior is consistent with the fact that S_{2-4} molecules instead of cyclo- S_8 exist in the composite, which leads to the reducing process starting from S_{2-4} to S^{2-} , avoiding the transition from S_8 to S_4^{2-} and resulting in the disappearance of Plateau-I. When charging, S/(CNT@MPC) also shows a single plateau at ~2 V, indicating that the space confinement of carbon micropores makes the S^{2-} in the S/(CNT@MPC) unable to grow into large S_{5-8} , but it can grow into small molecules of S_{2-4} that can be accommodated in the pores. The reversible redox reaction between S_{2-4} and S^{2-} is further confirmed by the cycling voltammetry of S/(CNT@MPC), which shows only one pair of reversible redox peaks (Figure S8). The reversible capacity of S/(CNT@MPC) is 1190 (476) mA·h/g, leading to a reasonable Coulombic efficiency of 71%, indicating the alleviation of the dissolution and shuttling problems of polysulfides, which is further confirmed by ex situ SEM observations of the counter electrodes of Li anodes in cycled Li-S batteries (Figure S9). Many micrometer-sized S-containing particles are found on the Li anode used in the Li-S/CB battery after only one GDC cycle (Figure S8a), while no S is detected on the Li anode used in the Li-S/(CNT@MPC) battery after 50 cycles at 0.1 C (Figure S8b). The confined S_{2-4} molecules in S/(CNT@MPC) exhibit much improved cycling stability compared with the cyclo- S_8 in S/CB (Figure 3b) due to the alleviation of the dissolution and shuttling problems of polysulfides. The reversible capacity of S/(CNT@MPC) is still 830 (332) mA·h/g after 50 cycles, while that of S/CB is <30 (12) mA·h/g.

When using a carbonate-based electrolyte of 1 M LiPF₆ in ethylene carbonate/dimethyl carbonate (1:1 wt%), the composite containing S_{2-4} still shows one GDC plateau but exhibits a higher lithium electroactivity (Figure 4a). An initial discharge capacity of 1670 (668) mA·h/g (Figure 4a) is obtained for S/(CNT@MPC) at 0.1 C, which is close to the theoretical capacity of sulfur (1675 mA·h/g), and much higher than that of S/CB (~573 (229) mA·h/g) under the same experimental conditions.

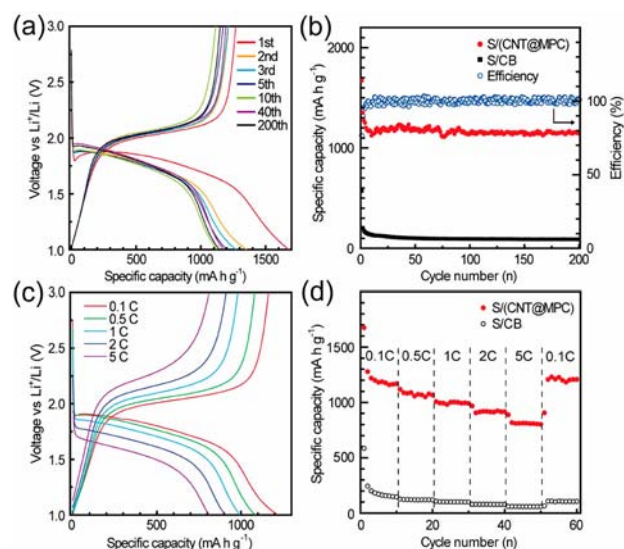


Figure 4. Electrochemical properties in carbonate-based electrolyte. (a) GDC voltage profiles of S/(CNT@MPC) at 0.1 C. (b) Cycling performance of S/(CNT@MPC) and S/CB at 0.1 C (blue circles show the Coulombic efficiency of S/(CNT@MPC)). (c) GDC voltage profiles of S/(CNT@MPC) at different discharge/charge rates. (d) Rate capabilities of S/(CNT@MPC) and S/CB.

To prove the space confinement of MPC on the generated Li₂S in carbonate electrolyte, both crystalline Li₂S powder and Li₂S/(CNT@MPC) composite after the first discharge process (discharge to 1 V) were sealed in a glass holder for Raman characterization, and their spectra were collected (Figure S7b). As can be seen, the crystalline Li₂S powder has a strong shift at 370 cm⁻¹; however, no additional peaks except for the D-band and G-band of amorphous carbon are found in the spectrum of Li₂S/(CNT@MPC), which proves the fine accommodation of the generated Li₂S in MPC without any crystalline Li₂S formed outside. The S/(CNT@MPC) shows a high reversible capacity of 1269 (508) mA·h/g and a high initial Coulombic efficiency of 76% in the first cycle (Figure 4a). They quickly stabilize at 1150 (460) mA·h/g and approach ~100% after several cycles. The S/(CNT@MPC) still delivers a reversible capacity of as high as 1142 (457) mA·h/g after 200 cycles, whereas the S/CB is only 90 (36) mA·h/g (Figure 4b). The results indicate the superior lithium electroactivity and cycling stability of the confined S_{2-4} in S/(CNT@MPC) compared with the cyclo- S_8 in S/CB.

The S_{2-4} in S/(CNT@MPC) also exhibits a superior high-rate capability. At a very high rate of 5 C (i.e., 8375 mA/g), S/(CNT@MPC) still exhibits a significant output voltage plateau at ~1.7 V, a high specific capacity of 800 (320) mA·h/g (~60 (24) mA·h/g for S/CB), a high Coulombic efficiency of 100%, and a small polarization of <0.6 V, indicating a remarkably improved high-rate capability (Figure 4c,d).

Carbonate-based solvents, such as ethylene carbonate and dimethyl carbonate, have been reported to be inappropriate for S_8 -based cathode materials.⁸ Due to their reactions with the large polysulfides (Li₂S_n, n = 5–8) formed at the first discharge plateau at ~2.4 V, sulfur cannot be fully reduced.⁸ However, it is the unique S_{2-4} molecules in S/(CNT@MPC) that make such an electrolyte workable. The compatibility of the carbonate electrolyte with the S/(CNT@MPC) cathode further confirms the different sulfur forms in the composite from the commonly reported S_8 -based cathode materials.

To investigate the structural stability of S/(CNT@MPC), TEM characterizations were performed on the S/(CNT@MPC) cathode after 200 cycles at 0.1 C in the carbonate electrolyte. As shown in Figure 2g, the S/(CNT@MPC) still maintains its cable-like structure with unchanged MPC layer and CNT core, demonstrating the robust structure of the composite. The elemental mapping results confirm the existence of uniformly distributed sulfur in the MPC layer (Figure 2j–l), and the ABF-STEM image taken from the MPC layer shows that the short-chain-like sulfur molecules are still accommodated in the carbon micropores (red circles in Figure 2i). After 200 cycles, the used S/(CNT@MPC) still contains 36.1 wt% S based on the EDX analysis (Figure S3b). The result further demonstrates the good stability of the confined S_{2-4} free of the problem of polysulfide dissolution into electrolyte during GDC cycles.

The outstanding electrochemical properties of the confined S_{2-4} molecules in S/(CNT@MPC) could be attributed to the following factors: First, the S_{2-4} molecules can avoid the transition from S_8 to S_4^{2-} during the initial Li uptake process, thereby preventing the formation of polysulfides (Li_2S_n , $n = 4-8$) upon discharging. Second, the space confinement of carbon micropores on sulfur leads to a favorable memory effect; viz., the in situ formed S^{2-} in Li_2S can only be oxidized to S_{2-4} rather than S_{5-8} , which also avoids the formation of polysulfides in the charging process. Therefore, the confined S_{2-4} can essentially solve the dissolution problem of polysulfides and account for the much improved cycling performance of S/(CNT@MPC). Third, the CNT core can serve as a metallizer for providing sufficient e^- for the redox reactions between Li^+ and S and hence improve the Li electroactivity.⁹ Finally, the carbon micropores of MPC could supply unperturbed Li^+ for the confined S_{2-4} to enhance the electrode reaction kinetics.¹⁰ The CNT core and the micropores of MPC form an efficient mixed-conducting 3D network for achieving the superior high-rate capability of S/(CNT@MPC).

In summary, we have successfully realized the metastable sulfur allotropes S_{2-4} via confining them in carbon micropores. These confined small S_{2-4} molecules exhibit a high Li electroactivity and a novel electrochemical behavior with a single output plateau at ~ 1.9 V, in contrast to the common cyclo- S_8 , and can essentially solve the critical problem of polysulfide dissolution in conventional Li–S batteries. The as-obtained S_{2-4} in S/(CNT@MPC) show a high specific capacity of 1670 (668) mA·h/g, an impressive cycling stability of 1149 (457) mA·h/g after 200 cycles, and a favorable high-rate capability of 800 (320) mA·h/g at 5 C. The success of the novel S cathode promises a new Li–S battery with higher energy density (785 W·h/kg based on anode and cathode) than state-of-the-art Li-ion batteries (theoretically 387 W·h/kg in a $LiCoO_2/C$ battery) for powering our future electronics. In view of the wide applications of sulfur such as fertilizers, medicines, fungicides, and cell nutrients, our discovery of these unusual small sulfur allotropes may trigger wide research interest in these fields as well.

■ ASSOCIATED CONTENT

Supporting Information

Detailed preparation methods for CNT@MPC, S/(CNT@MPC), and S/CB composites, their structural and electrochemical characterization, and theoretical calculation of various sulfur allotropes. This material is available free of charge via the Internet at <http://pubs.acs.org>.

■ AUTHOR INFORMATION

Corresponding Author

ygguo@iccas.ac.cn; wanlijun@iccas.ac.cn

Notes

The authors declare no competing financial interest.

■ ACKNOWLEDGMENTS

This work was supported by the National Key Project on Basic Research (Grant Nos. 2011CB935700 and 2012CB932900), the National Natural Science Foundation of China (Grant Nos. 51225204, 91127044, and 21121063), and the Chinese Academy of Sciences. The authors thank Prof. Y. Ikuhara and Dr. S. Tsukimoto for the ABF-STEM support, and Dr. Anmin Cao and Dr. B. Schumann for helpful discussions.

■ REFERENCES

- (1) (a) Armand, M.; Tarascon, J. M. *Nature* **2008**, *451*, 652. (b) Ji, X.; Lee, K. T.; Nazar, L. F. *Nat. Mater.* **2009**, *8*, 500. (c) Yuan, L. X.; Wang, Z. H.; Zhang, W. X.; Hu, X. L.; Chen, J. T.; Huang, Y. H.; Goodenough, J. B. *Energy Environ. Sci.* **2011**, *4*, 269. (d) Malik, R.; Zhou, F.; Ceder, G. *Nat. Mater.* **2011**, *10*, 587. (e) Zhu, Y.; Murali, S.; Stoller, M. D.; Ganesh, K. J.; Cai, W.; Ferreira, P. J.; Pirkle, A.; Wallace, R. M.; Cychosz, K. A.; Thommes, M.; Su, D.; Stach, E. A.; Ruoff, R. S. *Science* **2011**, *332*, 1537. (f) Meng, X.; Yang, X.-Q.; Sun, X. *Adv. Mater.* **2012**, *24*, 3589. (g) Chen, J.; Cheng, F. *Acc. Chem. Res.* **2009**, *42*, 713. (h) Li, J.-T.; Zhou, Z.-Y.; Broadwell, I.; Sun, S.-G. *Acc. Chem. Res.* **2012**, *45*, 485. (i) Wang, B.; Chen, J. S.; Wu, H. B.; Wang, Z.; Lou, X. W. *J. Am. Chem. Soc.* **2011**, *133*, 17146. (j) Dong, S. M.; Chen, X.; Gu, L.; Zhou, X. H.; Li, L. F.; Liu, Z. H.; Han, P. X.; Xu, H. X.; Yao, J. H.; Wang, H. B.; Zhang, X. Y.; Shang, C. Q.; Cui, G. L.; Chen, L. Q. *Energy Environ. Sci.* **2011**, *4*, 3502. (k) Cao, Y.; Xiao, L.; Sushko, M. L.; Wang, W.; Schwenzler, B.; Xiao, J.; Nie, Z.; Saraf, L. V.; Yang, Z.; Liu, J. *Nano Lett.* **2012**, *12*, 3783. (l) Chen, Z.; Augustyn, V.; Jia, X.; Xiao, Q.; Dunn, B.; Lu, Y. *ACS Nano* **2012**, *6*, 4319. (m) Abouimrane, A.; Dambournet, D.; Chapman, K. W.; Chupas, P. J.; Weng, W.; Amine, K. *J. Am. Chem. Soc.* **2012**, *134*, 4505. (n) Chiang, Y. M. *Science* **2010**, *330*, 1485. (o) Chen, Y.; Freunberger, S. A.; Peng, Z.; Bardé, F.; Bruce, P. G. *J. Am. Chem. Soc.* **2012**, *134*, 7952. (p) Weichert, K.; Sigle, W.; van Aken, P. A.; Jammnik, J.; Zhu, C.; Amin, R.; Acartürk, T.; Starke, U.; Maier, J. *J. Am. Chem. Soc.* **2011**, *134*, 2988.
- (2) Kim, H. S.; Arthur, T. S.; Allred, G. D.; Zajicek, J.; Newman, J. G.; Rodnyansky, A. E.; Oliver, A. G.; Boggess, W. C.; Muldoon, J. *Nat. Commun.* **2011**, *2*, 427.
- (3) Ji, X.; Nazar, L. F. *J. Mater. Chem.* **2010**, *20*, 9821.
- (4) (a) Hassoun, J.; Scrosati, B. *Angew. Chem., Int. Ed.* **2010**, *49*, 2371. (b) Hassoun, J.; Kim, J.; Lee, D.-J.; Jung, H.-G.; Lee, S.-M.; Sun, Y.-K.; Scrosati, B. *J. Power Sources* **2012**, *202*, 308. (c) Yang, Y.; McDowell, M. T.; Jackson, A.; Cha, J. J.; Hong, S. S.; Cui, Y. *Nano Lett.* **2010**, *10*, 1486.
- (5) (a) Yamin, H.; Peled, E. *J. Power Sources* **1983**, *9*, 281. (b) Kumaresan, K.; Mikhaylik, Y.; White, R. E. *J. Electrochem. Soc.* **2008**, *155*, A576. (c) Nelson, J.; Misra, S.; Yang, Y.; Jackson, A.; Liu, Y.; Wang, H.; Dai, H.; Andrews, J. C.; Cui, Y.; Toney, M. F. *J. Am. Chem. Soc.* **2012**, *134*, 6337.
- (6) (a) Elazari, R.; Salitra, G.; Garsuch, A.; Panchenko, A.; Aurbach, D. *Adv. Mater.* **2011**, *23*, 5641. (b) Zhang, B.; Qin, X.; Li, G. R.; Gao, X. P. *Energy Environ. Sci.* **2010**, *3*, 1531. (c) Hassoun, J.; Scrosati, B. *Adv. Mater.* **2010**, *22*, 5198. (d) Wang, J.; Chew, S. Y.; Zhao, Z. W.; Ashraf, S.; Wexler, D.; Chen, J.; Ng, S. H.; Chou, S. L.; Liu, H. K. *Carbon* **2008**, *46*, 229. (e) Jayaprakash, N.; Shen, J.; Moganty, S. S.; Corona, A.; Archer, L. A. *Angew. Chem., Int. Ed.* **2011**, *50*, 5904. (f) Wang, H.; Yang, Y.; Liang, Y.; Robinson, J. T.; Li, Y.; Jackson, A.; Cui, Y.; Dai, H. *Nano Lett.* **2011**, *11*, 2644. (g) Fu, Y.; Manthiram, A. *J. Phys. Chem. C* **2012**, *116*, 8910.
- (7) Guo, J. C.; Xu, Y. H.; Wang, C. S. *Nano Lett.* **2011**, *11*, 4288.
- (8) Gao, J.; Lowe, M. A.; Kiya, Y.; Abruña, H. D. *J. Phys. Chem. C* **2011**, *115*, 25132.
- (9) Cao, F.-F.; Guo, Y.-G.; Zheng, S.-F.; Wu, X.-L.; Jiang, L.-Y.; Bi, R.-R.; Wan, L.-J.; Maier, J. *Chem. Mater.* **2010**, *22*, 1908.
- (10) Guo, Y.-G.; Hu, J.-S.; Wan, L.-J. *Adv. Mater.* **2008**, *20*, 2878.